FUSION OF THREE OPTICAL SENSORS FOR NONDESTRUCTIVE DETECTION OF WATER CONTENT IN LETTUCE CANOPIES[**]

H. Y. Gao[*], H. P. Mao, X. D. Zhang, I. Ullah, X. H. Wei

School of Agricultural Engineering at Jiangsu University,
Zhenjiang 212013, China; e-mail: gaohy@ujs.edu.cn

Experiments were conducted to develop and assess a method by which the water content of a lettuce canopy can be nondestructively detected and estimated using a combination of spectra, RGB images, and canopy temperature. To this end, 130 lettuce samples grown in four different substrate water content levels were collected for data acquisition. In the spectroscopy procedure, five spectral intervals (380 variables) were selected by backward interval partial least squares and were further reduced to 48 wavelength variables, chosen using a genetic algorithm based on Savitzky–Golay smoothing and log (1/R) transformation. Then, 967, 1170, 1221, 1406, 1484, 1942, and 1985 nm optimum spectral variables were selected by the successive projection algorithm. Thirteen plant features were extracted from top- and front-view RGB images. These features comprised morphological, color, and textural features. An empirical crop water stress index was established based on dry and wet reference surfaces via thermal imagery. Subsequently, a principal component analysis was applied to the spectral variables and the image features, and an extreme learning machine was used to construct the multisensor and single-sensor models. The results show that the multisensor model had a correlation coefficient of prediction of 0.9018, which was found to be approximately 9.4 and 15.7% better than that of the spectral and image models. This work demonstrates that integrating spectra, RGB images, and canopy temperature with suitable algorithms offers a high potential for use in the nondestructive measurement of water content in lettuce, considerably improving accuracy over that using a single-sensor modality.

Keywords: spectrum, RGB images, canopy temperature, multi-sensors data fusion, nondestructive detection of water content.

ОПТИЧЕСКИЙ МЕТОД ОБНАРУЖЕНИЯ ВОДЫ В ЛИСТЬЯХ САЛАТА

H. Y. Gao[*], H. P. Mao, X. D. Zhang, I. Ullah, X. H. Wei

УДК 535.33:633.913.331

Школа сельскохозяйственной инженерии Университета Цзянсу,
212013, Чжэньцзян, Китай; e-mail: gaohy@ujs.edu.cn,

Предложен и экспериментально протестирован метод неразрушающего контроля содержания воды в листьях салата латук, основанный на использовании комбинации спектров, RGB-изображений и температуры растительного покрова. Для сбора данных отобрано 130 образцов салата, выращенных при четырех различных уровнях содержания воды в субстрате. Для спектроскопических измерений с помощью метода частичных наименьших квадратов, использующего алгоритм обратных интервалов, выбраны пять спектральных интервалов, включающих в себя 380 точек, число которых далее уменьшено до 48 с использованием генетического алгоритма, основанного на сглаживании Савицкого–Голея и логарифмическом (1/R) преобразовании. С помощью метода последовательных проекций выбраны оптимальные для измерения длины волн 967, 1170, 1221, 1406, 1484, 1942 и 1985 нм. Тринадцать морфологических, цветовых и текстурных особенностей растений выявлены

из RGB-изображений – фронтального и вида сверху. На основе сопоставления тепловых изображений исследуемых образцов с таковыми для сухих и влажных эталонных поверхностей эмпирически установлен индекс водного стресса. К спектральным данным и характеристикам изображения применен анализ главных компонент, причем для построения моделей с несколькими и одним сенсорами использован метод экстремального машинного обучения. Результаты показывают, что модель с несколькими сенсорами имеет коэффициент корреляции 0.9018, который на ~9.4 и 15.7% лучше, чем у спектральной модели и модели изображений.

Ключевые слова: *спектр, RGB-изображения, температура растительного покрова, объединение данных множества сенсоров, неразрушающий контроль содержания воды.*

Introduction. Lettuce is a leaf-edible vegetable that is widely cultivated throughout the world and plays an important role in human nutrition and diet. China's lettuce production accounted for more than half of the world's, and irrigation is one of the main factors affecting lettuce yield. Lettuce is extremely sensitive to drought because of its shallow root system, multiple leaves, and large leaf area [1]. Water stress causes reductions in the photochemical activity of pigments, absorption of nutrients, and nutrient transport from roots to shoots [2]. Hence, plant response to water stress is expressed by a variety of physiological (e.g., stomatal closure, chlorophyll status, and leaf water content) and biophysical (e.g., leaf and canopy structure, leaf area, plant height, dry weight, biomass, and yield) traits [3]. Some of these traits are internal reactions, while some are external manifestations. Thus, it is desirable to use a multisensor-based, multiple plant feature extraction method for lettuce canopy water content monitoring.

With the ever-increasing tendency to employ automation in agricultural operations and the development of precision agriculture concepts, it is desirable to develop non-destructive technologies and applications to monitor plant parameters. Spectra, RGB images, and thermal imagery are effective technologies for drought monitoring because they facilitate the natural integration of various types of vegetation information into agricultural drought indicators, which are otherwise difficult to measure through direct field observations [4].

Spectroscopy is being increasingly used for ecophysiological studies because of its rapidity, simplicity, and nondestructive nature. In previous scientific research, the plant water status of different species has been predicted by spectrometry. Danson et al. [5] used six wavebands of the maxima and minima of water absorption, centered at 975, 1175, 1450, 1650, 1950, and 2250 nm, and the first spectral derivative to determine leaf water content. Clevers et al. [6] used the features at around 970 and 1200 nm to investigate the derivative spectra, maximum band depth, and area under curve algorithms, and thereby map the leaf water content.

An RGB image, which has been used to detect early signs of crop water stress considering that they allow fast and nondestructive phenotyping in plants, has the potential to detect trends in plants before human visual detection is performed. Hendrawan and Murase [7] used machine vision to sense the water content in cultured Sunagoke moss. Their image features consisted of eight color features (CFs), three morphological features (MFs), and 90 textural features (TFs), and the minimum average prediction means square error achieved was 1.75×10^{-3}. Zhuang et al. [8] presented a model to detect the water stress of maize in the early stages. They extracted 14 CFs and TFs from the RGB image, and the accuracy of the detected water stress reached 90.39%.

In addition to spectroscopy and RGB imaging techniques, recent developments in thermal infrared imaging (TIR) technology have focused on using canopy temperature (T_c) measurements for realizing applications in variable rate irrigation [9]. One of the most commonly used methods for normalizing T_c as an indicator of plant water status is the crop water stress index (CWSI), and its use in irrigation management has been substantiated [10]. Adeyemi et al. [11] demonstrated the empirical CWSI ($CWSI_E$) approach that can be deployed as an irrigation monitoring tool for greenhouse cultivated lettuce crops.

At present, many approaches employ single sensor technology for the detection of plant water status. We proposed three multisensor data fusion schemes to implement the non-destructive detection of water status in lettuce canopy. The proposed fusion approach could utilize the combined information of spectra, RGB images, and T_c sensors to develop a novel and comprehensive data fusion method based on multiple sensors. This approach could improve irrigation accuracy substantially.

Materials and methods. *Plant material and growing conditions.* Lettuce (*Lactuca sativa*, Italian) was obtained from Woshu Seeds Co. Ltd., Nanjing, China. Experiments were performed in a greenhouse located at Jiangsu University in China (32.11N, 119.27E) in the spring from 27 April to 15 June 2017. Lettuce seedlings with five true leaves were transplanted individually into plastic pots filled with perlite. For the irrigation control treatment, irrigation amounts were 25% (T1), 50% (T2), 75% (T3), and 100% (T4), which were

determined based on the water-holding capacity of the substrate. The pots were weighed before each irrigation schedule, and a reduced amount of water was added to the pots to maintain the four irrigation control treatments. The Yamasaki lettuce recipe was used for lettuce growth. The lettuce roots were always provided with a fixed water content by a self-developed timed irrigation and collection system [12]. The canopy reflectance, images, and thermal infrared imaging data were recorded 15 days after transplanting.

Spectra data acquisition. The canopy reflectance was acquired using a portable analysis spectral devices (ASD) FieldSpec® Pro Spectrometer, which was provided with a spectral range of 350–2500 nm using a custom-made optical box [13]. The spectrometer was equipped with three sensors with a spectral sampling of 3, 10, and 10 nm. The built-in spectral resolution output of the data from the ASD operating system was 1 nm along the entire spectrum. Spectral measurements were taken using a fiber optic cable with a 25° field of view, which was placed 18 cm above the canopy. A 50-W halogen lamp was used for producing radiation. The instrument was periodically calibrated in terms of spectral reflectance using a standard white reference panel. Five replicate spectral measurements were taken for each sample and noise reduction was achieved by averaging the spectra.

Computer vision data acquisition. The images of the lettuce canopy were taken using two digital cameras (EOS 400D, Canon Inc.) placed in the custom-made optical box. A white background plate was fixed to the lettuce roots and a normal graph paper was set at the same height as the lettuce canopy. One of the cameras was positioned above the top of the canopy using a tripod, and another camera was positioned at the front of the canopy to obtain the front view images. The aperture priority mode was selected. The camera aperture was set to f/8, and ISO was set to 100. The digital images were stored in JPEG format.

Thermal infrared imaging data acquisition and $CWSI_E$ calculation. The $CWSI_E$ was intended as a tool for detecting the water status of plants around noon, which corresponds to the period of peak plant transpiration [11]. Khorsandi et al. [14] used infrared thermography for detecting Tc in sesame under greenhouse conditions from 11:00 to 14:00 h. Hence, to better determine the canopy temperature acquisition time, an extended period between 8:00 and 16:00 h was explored during this study according to reference [11]. Infrared images were taken with handheld infrared thermography (Thermocamera Fluke Ti25, Fluke Corporation, USA) with a resolution of 160×120 pixels, which operates in the waveband range of 7.5–14 μm. The camera had a thermal resolution of 0.1°C, and the accuracy of the absolute temperature measurement was less than ±2°C. The emissivity for the canopy was set at 0.96, which is quoted for plant leaf by Jones [15].

The $CWSI_E$ uses two baseline temperatures: the temperature of a well-watered canopy, referred to as the lower limit baseline temperature (T_{wet}), and the temperature of a non-transpiring canopy, referred to as the upper limit baseline temperature (T_{dry}). Artificial wet and dry reference surfaces were created. For the T_{wet} measurement, the lettuce canopy was sprayed on both sides with water as a wetting agent approximately 1 min before the imaging, whereas for the T_{dry} measurement, the canopy was covered in petroleum jelly (vaseline) on both sides [16]. The $CWSI_E$ is defined as [17]

$$CWSI_E = (T_c - T_{wet})/(T_{dry} - T_{wet}),$$

where T_c is the actual canopy surface temperature (°C), T_{wet} is T_c of a non-water-stressed canopy (°C), and T_{dry} is T_c of a non-transpiring canopy (°C).

For the canopy water content measurement, the leaves were cut and weighed on an analytical balance. Later, the leaves were placed in paper bags and dried at 70°C in an oven until a constant mass was reached. Next, each sample was weighed and the water content was calculated, according to the methodologies of [18]:

$$CWC = [(FW - DW)/DW] \times 100\%,$$

where CWC is the canopy water content, FW is the canopy fresh weight (g), and DW is the oven-dry weight of the same sample (g).

Spectral transformation. Appropriate spectrum preprocessing and selection of informative variables (spectral wavelengths) are essential to improve the performance of the model and reduce model complexity. The raw reflectance spectra were reduced to 400–2450 nm to eliminate the noise at the edges of each spectrum (Fig. 1a) [19]. To eliminate multiple scattering, high-frequency noise, and other interferences that can reduce the performance of the model, Savitzky–Golay smoothing (nine smoothing points) [20] and log (1/R) (where R is the reflectance) [21] were used for spectral preprocessing (Fig. 1b).

Splitting the calibration and prediction subsets. All the samples were divided into two subsets. The first subset was called the calibration set, in which all the samples were used for modeling, and the second subset was called the prediction set, in which all the samples were used to test the robustness of the final model. The joint *x-y* distance (SPXY) algorithm [22] was used for dividing the sample subsets, which considered

the weights of x-matrix (canopy spectral reflectance) and y-vector (CWC) at the same time. The calibration set contained 90 samples and the remaining 40 samples comprised the prediction set. The results of water content analysis in the calibration set and the prediction set are shown in Table 1. The performance of the final model was evaluated using the root MSE of cross-validation (RMSECV) and the correlation coefficient (R_c) in the calibration set, and the root MSE of prediction (RMSEP) and the correlation coefficient (R_p) in the prediction set.

TABLE 1. Results of Water Content Analysis in the Calibration Set and the Prediction Set

Data Set	Number samples	Minimum of water content, %	Maximum of water content, %	Mean, %	Standard deviation, %
Calibration set	90	1037	2845	1802	559
Prediction set	40	1207	2740	1852	436

Results and discussion. *Extraction of optimum wavelengths.* Because high redundancy may decrease the estimation capability and computing efficiency of the model, the optimum spectral intervals were selected by using an improved version of the interval partial least squares (iPLS) algorithm, called the backward iPLS (BiPLS) algorithm [23]. In this study, the full spectrum (400–2450 nm) was divided into 10–40 intervals. The optimum BiPLS model was obtained with 27 intervals. The best intervals chosen by BiPLS were 8, 11, 14, 15, and 21, and these efficient spectral intervals corresponded to 932–1007, 1160–1235, 1388–1463, 1464–1539, and 1920–1995 nm. There were 380 variables in total (Fig. 1d).
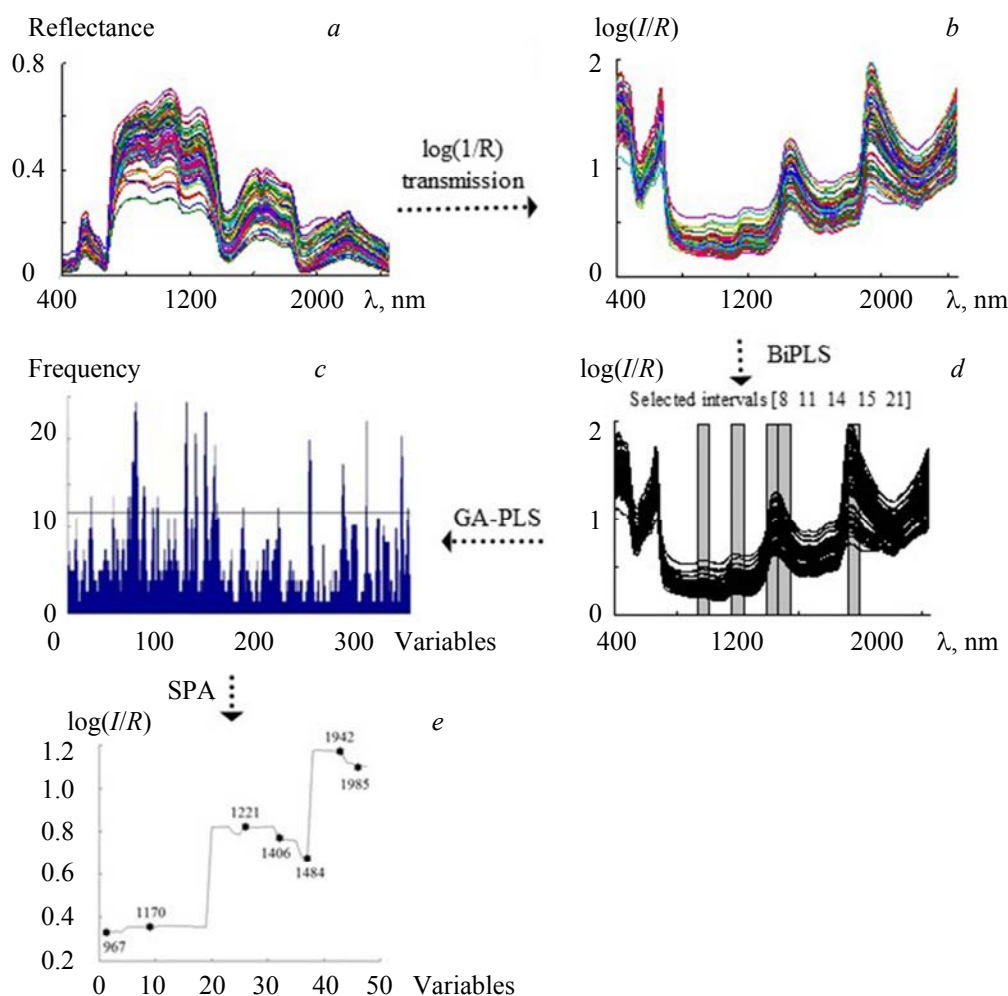

Fig. 1. The spectral transformation and extraction process of optimum wavelengths.

The genetic algorithm PLS (GA-PLS) [24] was used for variable selection from 380 spectral variables. The number of genes in each chromosome was equal to the number of samples. The crossover rate was 0.5, and the mutation rate was 0.01. The termination condition was reached when 100 generations were run. GA-PLS was performed 10 times to remove random effects. Figure 1c shows the histogram of the selected frequency of each variable involved in the PLS model. A variable was included if its frequency of selection reached or exceeded the horizontal line. Thus, 48 variables with a higher selected frequency were determined.

However, the collinear wavelengths remained in the 48 variables. To obtain optimum spectral variables, the successive projections algorithm (SPA) – a variable selection technique aimed at reducing collinearity problems [25] – was used to further eliminate the collinear variables from the variables selected by BiPLS and GA-PLS. The SPA was applied to the dataset, and seven variables were selected, specifically, 967, 1170, 1221, 1406, 1484, 1942, and 1985 nm (Fig. 1e).

Extraction of optimum image feature variables. Water deficiency causes obvious changes in plant color, texture, and morphology. In this study, all the top view images (Fig. 2a) and front view images (Fig. 3a) were processed by using threshold segmentation and by applying the "2G-R−B" index to extract the lettuce target. The threshold was set as 0.2 based on experimentation. Then a binary image was obtained (Figs. 2b and 3b) in which the lettuce canopy was the white foreground. The white pixels of the binary image were converted to transparent, and hence the background was covered by all black pixels. To better exhibit the edge of the lettuce canopy, Figs. 2c and 3c have white backgrounds. Then they were transformed into the HSI color mode.
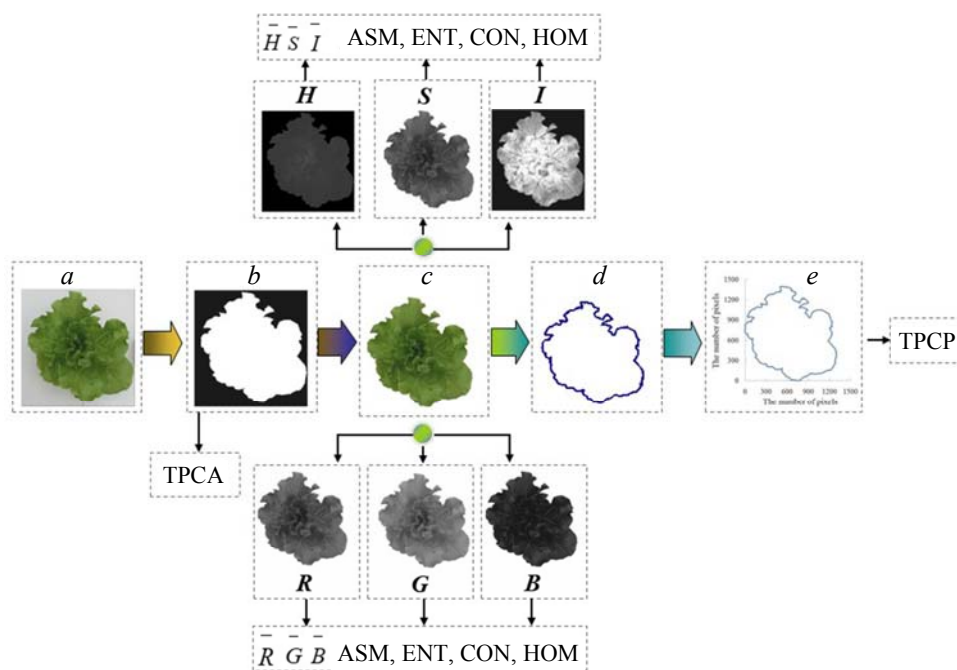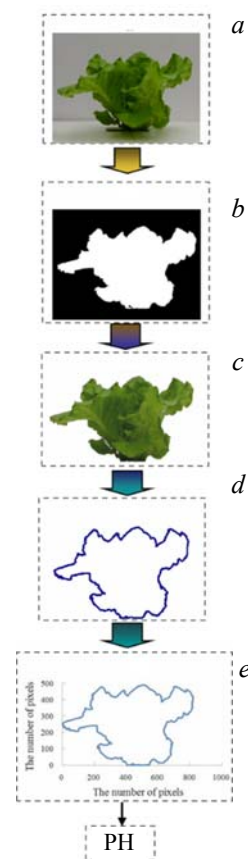

Fig. 2. Processing of the top view images.

Fig. 3. Processing of the front view images.

The red mean value ($\bar{R}$), green mean value ($\bar{G}$), blue mean value ($\bar{B}$), hue mean value ($\bar{H}$), saturation mean value ($\bar{S}$), and luminance mean value ($\bar{I}$) were extracted from each color space. They were calculated according to the following equation:

$$CFs = \frac{1}{M}\sum_{i=1}^{M} C,$$

where M is the total number of pixels and C is the color value of every pixel in the image (only the lettuce region; the background was ignored). The CFs can be defined as the following range: $\bar{R}[0,255]$, $\bar{G}[0, 255]$, $\bar{B}[0, 255]$, $\bar{H}[0, 360°]$, $\bar{S}[0, 1]$, and $\bar{I}[0, 1]$.

Texture analysis was conducted using the color co-occurrence matrix (CCM) method, which has been reported to successfully predict water content in plants. The CCM procedure consists of three primary mathematical processes. (1) $CCM_{R,G}$, $CCM_{R,B}$, $CCM_{G,B}$, $CCM_{H,S}$, $CCM_{H,I}$, and $CCM_{S,I}$ were generated from RGB and HSI images. (2) Four Haralick TFs—angular second moment (ASM), entropy (ENT), contrast (CON), and homogeneity (HOM)—were extracted from the CCM; these TFs were the most significant features correlated with plant health [26]. (3) The mean values of ASM, ENT, CON, and HOM regarded as TFs.

The top projected canopy area (TPCA) was a key factor in crop growth [27], which was obtained by dividing the number of white pixels by the conversion factor previously determined. The Roberts, Sobel, Laplacian, Gaussian, Canny, and Zero-cross edge detector algorithms [28] were applied to extract the top projected canopy perimeter (TPCP). The comparison showed that the Canny edge detector was especially suitable for the images (Figs. 2d,e) because the test on the images indicated that the edge detection by this method not only contained fewer pixels but also had a good closeness and true edges. The "2G-R−B" index and Canny edge detector were used to extract the plant height (PH) from the front view images (Figs. 3d, e). The TPCA, TPCP, and PH were calculated according to the following equations:

$$\mathrm{TPAF} = N_L/f_1, \ \mathrm{TPCP} = N_i/\sqrt{f_1}, \ \mathrm{PH} = N_H/\sqrt{f_2},$$

where N_L is the total number of pixels in the lettuce area, f_1 is the number of pixels per unit area (1 cm^2) in the top view images, N_P is the total number of pixels on the outer edge, N_H is the total number of pixels in the height direction, and f_2 is the number of pixels per unit area (1 cm^2) in the front view images.

Thus, after following the image processing and feature extraction process outlined above, 13 image features (6 CFs, 4 TFs, and 3 MFs) were available to estimate the water content in each lettuce sample.

Diurnal dynamics of CWSI$_E$. The thermal infrared images of rectangular regions of interest (ROI) were captured from 8:00 to 16:00 h (local standard time) at intervals of 1 h under clear skies when the sun was unobscured by clouds. The mean temperature of ROI was calculated as T_c. The results show that T_c increased first and decreased afterward in the day and that the highest temperature occurred around noon; T_c increased with increasing T_a and SR and with decreasing RH, and the relationship of T_c and T_a had a significant positive correlation. The time-varying $T_c - T_a$ values were calculated, which first increased and then decreased afterward on a sunny day; the maximum $T_c - T_a$ occurred at 13:00.

Then, the CWSI$_E$ values were calculated. With increase in irrigation, the CWSI$_E$ value decreased gradually, the diurnal course of CWSI$_E$ of T4 lettuce stayed at a relatively constant and low level, and the diurnal course of CWSI$_E$ of T1 lettuce increased until 13:00 h and decreased after that, following the dynamics of evaporative demand. The conclusions were consistent with the results of the references [11, 29].

Plant water stress assessment using multisensor data. Thus far, there were 21 variables for establishing a prediction model in lettuce canopy, thereby making the model complex. Hence, principal component analysis (PCA) [30] was implemented on the seven spectral variables and 13 image features, which led to the identification of three principal components (PCs) from the seven spectral variables and four PCs from the 13 image features. The cumulative variance contribution rate reached 99.52 and 98.24% according to the PCA method. The fusion model retained eight variables.

To achieve the best performance for predicting the water content in lettuce, extreme learning machine (ELM) algorithms were adopted to develop a detection model, and they were used for nonlinear multivariate data analysis [31]. The input variables were three spectral PCs, four image PCs, and one CWSI$_E$ value, and the output variable was the CWC. In the process of ELM modeling, the neuron number was selected by trial and error; values from 5 to 90 (90 being the number of samples in the calibration set) were considered at intervals of 5. Finally, the optimum ELM model for the water content was obtained with 50 hidden nodes and with RMSECV = 125%, R_c = 0.9412, RMSEP = 157%, and R_p = 0.9018. The arrangement leading up to the ELM modeling is shown in Fig. 4, and a scatter plot showing the correlation between predicted and measured water content in the prediction set is shown in Fig. 5.
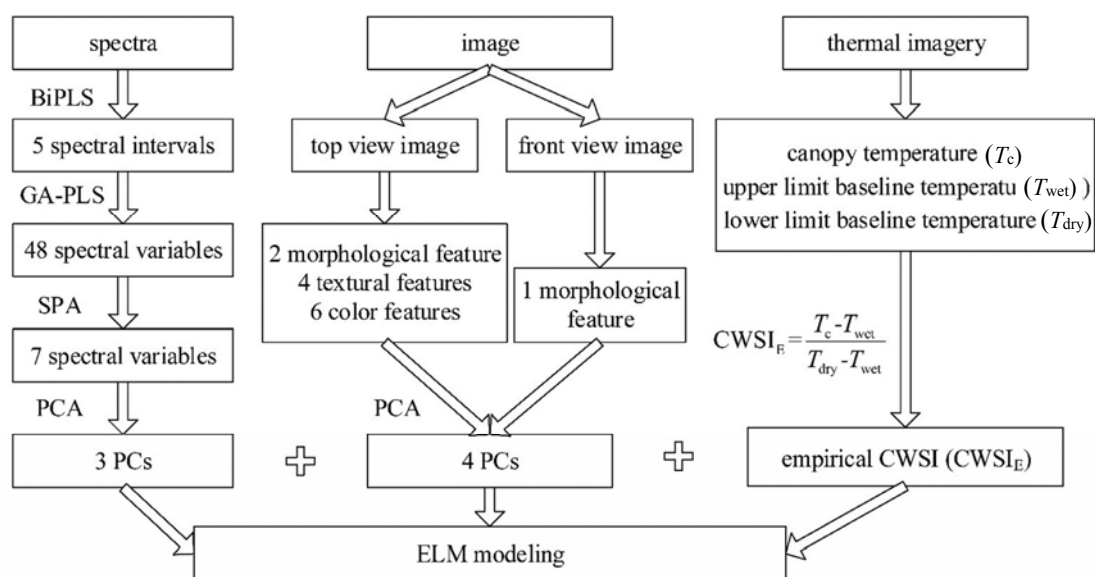
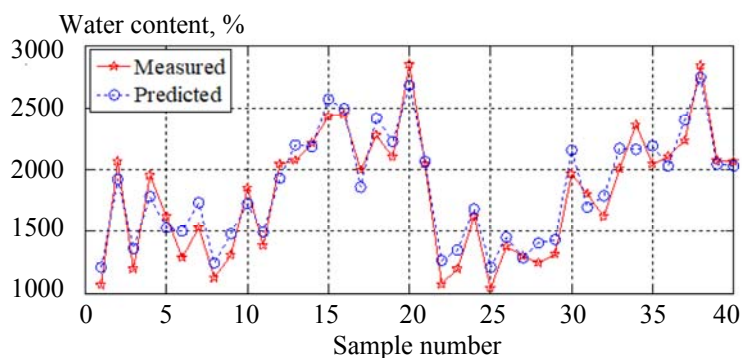Fig. 4. Arrangement for extreme learning machine (ELM) modeling.

Fig. 5. Reference measured value versus predicted value in the prediction sets.

Comparative analysis of single-sensor and multisensor models. As listed in Table 2, the models based on spectral and image data alone have been established by the ELM algorithm. The results showed that the multisensor model was the preferred modality, which was indicated by the higher R_P and lower RMSEP. The accuracy was approximately 9.4 and 15.7% better than that of the spectral and image models, respectively. These results can be attributed to the following reasons.

TABLE 2. Comparison of Results Based on Different Sensors

Models	Variables	Calibration set		Prediction set	
		RMSECV, %	R_c	RMSEP, %	R_p
Spectral data	7	162	0.8542	197	0.8243
Image data	13	198	0.8109	238	0.7794
Fusion data	8	125	0.9412	157	0.9018

Plants under different stress conditions may nevertheless show similar external symptoms [26]. Accordingly, a single inspection technique can only describe changes in one particular aspect. For instance, RGB images can document a plant's spatial information, and spectroscopy can identify or detect a plant's chemical properties [13]. When water stress occurs, the chemical properties of lettuce change earlier than the external characteristics. This is mainly due to the fusion of internal chemicals causing changes in external mor-

phology. Hence, the accuracy of the spectral model is superior to that of the image model. The spectral model accuracy is approximately 5.6% better than that of the image model. Canopy light reflectance properties based mainly on the absorption of light at a specific wavelength are associated with specific plant characteristics. Water molecules in the canopy weakly absorb electromagnetic energy in the VNIR and strongly absorb in the SWIR [32]. The characteristic wavelengths are located at 967, 1170, 1221, 1406, 1484, 1942, and 1985 nm, which is related to the C-H stretch and O-H bend overtone [33]. This makes sense because the CWC in lettuce is high.

Previous studies have shown that T_c has been accepted as an indicator of crop water stress because plants close their leaf stomata when they experience water stress, thereby lowering stomatal conductance, reducing transpiration, and increasing leaf temperatures [34]. However, Tc is influenced by the leaf angle and leaf dimension at the leaf level and is strongly impacted by the canopy height and structure at the canopy level [35, 36]. It does not account for changes in photosynthetic pigments in water-stressed crops [37] and is limited in estimating plant water status due to variations in environmental temperature and humidity [38]. Therefore, the three sensors have different thematic roles and are complementary. The detection accuracy of the model can be significantly improved based on the fusion of spectra, RGB images, and T_c.

Conclusions. In this study, non-destructive detection techniques for evaluating the water content in lettuce canopy were investigated, including spectra, RGB images, and T_c. Subsequently, seven optimum spectral variables (967, 1170, 1221, 1406, 1484, 1942, and 1985 nm) were selected from 2151 wavelengths using the BiPLS-GA-SPA method, which were significantly correlated with the water content of lettuce canopy. Second, six CFs, four TFs, and three MFs were extracted from the top and front view images of lettuce canopies. Third, the $CWSI_E$ model was established by TIR imaging. Finally, three ELM models based on single and multiple sensor modalities were established, and the analysis of their respective results indicated that the model based on spectra is superior to the one based on image data, and that the model based on fusion is superior to the model based on a single sensor modality. As such, the detection accuracy was significantly improved by the multisensor fusion method.

REFERENCES

1. Ü. Kızıl, L. Genç, M. İ. Nalpulat, D. Ş. Apolyo, M. Mirik, *Zemdirbyste*, **99**, 409–418 (2012).
2. A. M. H. Elmetwalli, A. N. Tyler, P. D. Hunter, C. A. Salt, *Remote Sens. Lett.*, **3**, 363–372 (2012).
3. M. El-Bially, H. Saudy, I. El-Metwally, M. Shahin, *Agric. Water Manage.*, **208**, 132–139 (2018).
4. N. Sanchez, A. Gonzalez-Zamora, J. Martinez-Fernandez, M. Piles, M. Pablos, *Agric. Meteorol.*, **259**, 141–153 (2018).
5. F. M. Danson, M. D. Steven, T. J. Malthus, J. A. Clark, *Int. J. Remote Sens.*, **13**, 461–470 (1992).
6. J. G. P. W. Clevers, L. Kooistra, M. E. Schaepman, *Int. J. Appl. Earth Obs. Geoinform.*, **12**, 119–125 (2010).
7. Y. Hendrawan, H. Murase, *Expert Syst. Appl.*, **38**, 14321–14335 (2011).
8. S. Zhuang, P. Wang, B. Jiang, M. S. Li, Z. H. Gong, *Comput. Electron. Agric.*, **140**, 461–468 (2017).
9. B. A. King, K. C. Shellie, *Comput. Electron. Agric.*, **145**, 122–129 (2018).
10. E. G. Kullberg, K. C. DeJonge, J. L. Chavez, *Agric. Water Manage.*, **179**, 64–73 (2017).
11. O. Adeyemi, I. Grove, S. Peets, Y. Domun, T. Norton, *Comput. Electron. Agric.*, **153**, 102–114 (2018).
12. H. Y. Gao, H. P. Mao, X. D. Zhang, *Zemdirbyste*, **102**, 51–58 (2015).
13. H. P. Mao, H. Y. Gao, X. D. Zhang, F. Kumi, *Sci. Hortic.*, **184**, 1–7 (2015).
14. A. Khorsandi, A. Hemmat, S. A. Mireei, R. Amirfattahi, P. Ehsanzadeh, *Agric. Water Manage.*, **204**, 222–233 (2018).
15. H. G. Jones, *Application of Thermal Imaging and Infrared Sensing in Plant Physiology and Ecophysiology*, Elsevier, London, 107–163 (2004).

16. P. R. Petrie, Y. N. Wang, S. Liu, S. Lam, M. A. Whitty, M. A. Skewes, *Biosyst. Eng.*, **179**, 126–139 (2019).

17. S. B. Idso, R. D. Jackson, P. J. Pinter Jr., R. J. Reginato, J. L. Hatfield, *Agric. Meteorol.*, **24**, 45–55 (1981).

18. P. Ceccato, S. Flasse, S. Tarantola, S. Jacquemoud, J. M. Gregoire, *Remote Sens. Environ.*, **77**, 22–33 (2001).

19. Y. Özyiğit, M. BiLgen, *J. Agric. Sci. Technol.*, **15**, 1537–1545 (2013).

20. A. Savitzky, M. J. E. Golay, *Anal. Chem.*, **36**, 1627–1639 (1964).

21. T. Shi, Y. Chen, H. Liu, J. Wang, G. Wu, *Appl. Spectrosc.*, **68**, 831–837 (2014).

22. R. K. H. Galvão, M. C. U. Araujo, G. E. José, M. J. C. Pontes, E. C. Silva, T. C. B. Saldanha, *Talanta*, **67**, 736–740 (2005).

23. R. Leardi, L. Nørgaard, *J. Chemometr.*, **18**, 486–497 (2004).

24. R. Leardi, *J. Chemometr.*, **14**, 643–655 (2010).

25. M. C. U. Araujo, T. C. B. Saldanha, R. K. H. Galvao, T. Yoneyama, H. C. Chame, V. Visani, *Chemometr. Intell. Lab. Syst.*, **57**, 65–73 (2001).

26. D. Story, M. Kacira, C. Kubota, A. Akoglu, L. An, *Comput. Electron. Agric.*, **74**, 238–243 (2010).

27. T. Hang, N. Lu, M. Takagaki, H. P. Mao, *Sci. Hortic.*, **252**, 113–120 (2019).

28. F. Bachofer, G. Queneherve, T. Zwiener, M. Maerker, V. Hochschild, *Eur. J. Remote Sens.*, **49**, 205–224 (2016).

29. N. Agam, Y. Cohen, J. A. J. Berni, V. Alchanatis, D. Kool, A. Dag, U. Yermiyahu, A. Ben-Gal, *Agric. Water Manage.*, **118**, 79–86 (2013).

30. F. R. S. Karl Pea, *J. Sci.*, **2**, 559–572 (1901).

31. G. B. Huang, D. H. Wang, Y. Lan, *Int. J. Mach. Learn. Cybern.*, **2**, 107–122 (2011).

32. S. Ullah, A. K. Skidmore, A. Ramoelo, T. A. Groen, M. Naeem, A. Ali, *ISPRS-J. Photogramm. Remote Sens.*, **93**, 56–64 (2014).

33. I. Torres, M. T. Sanchez, M. Benlloch-Gonzalez, D. Perez-Marin, *Biosyst. Eng.*, **180**, 50–58 (2019).

34. D. L. Mangus, A. Sharda, N. Q. Zhang, *Comput. Electron. Agric.*, **121**, 149–159 (2016).

35. W. H. Maes, K. Steppe, *J. Exp. Bot.*, **63**, 4671–4712 (2012).

36. Z. Thungo, H. Shimelis, A. O. Odindo, J. Mashilo, *Acta Agric. Scand. Sect. B-Soil Plant Sci.*, **70**, 177–194 (2020).

37. P. J. Zarco-Tejada, V. Gonzalez-Dugo, L. E. Williams, L. Suarez, J. A. J. Berni, D. Goldhamer, E. Fereres, *Remote Sens. Environ.*, **138**, 38–50 (2013).

38. S. Chung, L. E. Breshears, J.-Y. Yoon, *Comput. Electron. Agric.*, **154**, 93–98 (2018).